

Effects of woven textures on the mechanical and shape memory properties of epoxy-based shape memory polymer composites

Guangqing Ming^a, Mingming Xu^b, Fengfeng Li^{c,*}, Chengjun Zeng^c, Wei Zhao^c, Liwu Liu^c, Yanju Liu^c, Jinsong Leng^{a,*}

^a Center for Composite Materials and Structures, Harbin Institute of Technology, P.O. BOX 3011, No. 2 Yikuang Street, Harbin 150080, People's Republic of China

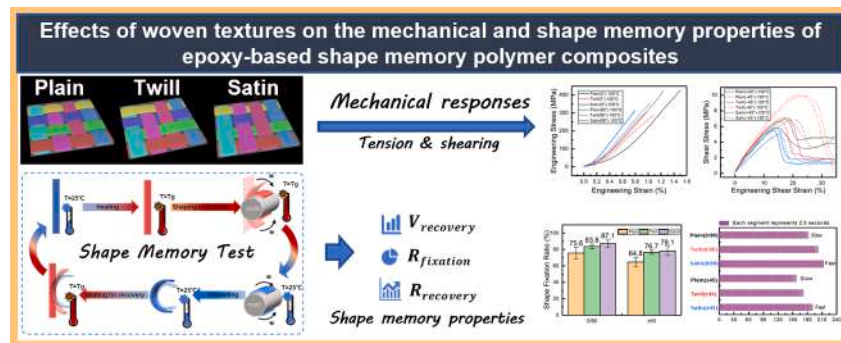
^b School of Science, Harbin Institute of Technology (Shenzhen), Shenzhen 518055, People's Republic of China

^c Department of Astronautical Science and Mechanics, Harbin Institute of Technology, P.O. Box 301, No. 92 West Dazhi Street, Harbin 150001, People's Republic of China

HIGHLIGHTS

- Woven fabrics improve mechanical properties of SMP.
- Woven textures induce anisotropic mechanical properties.
- Better shape memory in (0/90) than (± 45) direction for WFR-SMPCs.
- Deformation patterns vary between (0/90) and (± 45) directions.

GRAPHICAL ABSTRACT



ARTICLE INFO

Keywords:

Shape memory polymer
Woven fabric reinforced composites
Woven texture
Mechanical testing

ABSTRACT

Woven fabrics are widely employed to enhance the mechanical properties and shape memory performance of shape memory polymers (SMPs). Although prior research has extensively investigated the effects of fiber fraction and laminate architectures on the thermomechanical properties of woven fabric reinforced shape memory polymer composites (WFR-SMPCs), the mechanistic understanding of mesoscale architectural features, particularly how woven textures influence the mechanical properties and shape memory behavior of SMPCs, remains inadequately explored. This investigation pioneers a mesostructure-driven design paradigm, correlating woven textures with shape memory anisotropy through mechanical testing and shape memory performance test. Three types of WFR-SMPCs were created using different woven carbon fiber fabrics (plain, twill, and satin) combined with an epoxy-based SMP. Microstructure analyses of these fabrics and their composites were performed. Uniaxial tensile tests explored the mechanical behavior and failure mechanisms of WFR-SMPCs in both fixed and programmable states, thereby assessing the impact of different woven textures on their mechanical properties. Additionally, bending deformation-recovery experiments assessed the shape memory performance, revealing how weave texture influences this characteristic. The experimental results indicated that woven fabric reinforcement markedly improves the mechanical properties of SMP. Variations in tow interlacing across weave

* Corresponding authors.

E-mail addresses: lifengfeng@hit.edu.cn (F. Li), lengjs@hit.edu.cn (J. Leng).

types led to differing mechanical properties and shape memory performance in both (0/90°) and (±45°) orientations. This research offers critical insights for optimizing the design and application of WFR-SMPCs in engineering contexts.

1. Introduction

Shape memory polymers (SMPs) are smart stimuli-responsive materials capable of a dual-shape memory cycle [1]. For thermally-induced SMPs, thermomechanical programming involves deforming the material above its glass transition temperature (T_g) under external force. Subsequently, cooling below T_g fixes the temporary shape through vitrification or crystallization. When reheated above T_g , the material can recover its original shape as the entropic energy stored in the deformed polymer chains is released, driving molecular realignment. This transition between programmed and permanent states, termed the shape memory effect (SME), arises from the dynamic interaction of a crosslinked network (maintaining the permanent shape) and reversible phase transitions (storing the temporary shape). SMPs have been widely applied in various fields such as aerospace, biomedicine, and smart textiles due to their unique shape memory effects [2–4]. However, the inherent mechanical properties of pure SMPs are often insufficient to meet specific application requirements. To enhance their performance, researchers have begun exploring the combination of SMPs with reinforcing materials such as particles and fibers, leading to the creation of shape memory polymer composites [5–10]. Woven fabrics, as a common fibrous reinforcement, are extensively used in combination with SMPs to form woven fabric reinforced shape memory polymer composites (WFR-SMPCs) due to their good processability and excellent mechanical properties [11–15].

Studies on WFR-SMPCs have shown that factors such as the laying angle, number of layers, and tow count of the woven fabric can significantly affect the macroscopic mechanical properties of the composite material. Liu et al. designed WFR-SMPC deployable hinges and discussed the impact of the number of woven layers on the hinge's recovery moment and deployment stiffness [16]. Fang et al. employed a combination of numerical simulation and experimental testing to compare the mechanical properties of WFR-SMPCs with different tow counts, revealing the mechanism by which tow count affects the composite's mechanical properties [17]. Qu et al. utilized a multi-scale modeling method to the mechanical behaviour analysis of composite materials, including the damage mode analysis of 3D stitched composites [18] and the stress distribution of WFR-SMPC under in-plane shear mode [19]. Notably, different woven textures possess varying degrees of compliance, which can influence the deformation behavior of the fabric. Boisse and Peng et al. have studied the anisotropic mechanical behavior of woven fabric composites under large deformations during stamping processes, predicting the fabric's deformation over double-dome mold through shear deformation experiments [20,21]. Asadi et al. examined the structural stability of different fabrics from the perspective of inter-yarn friction and woven texture [22]. However, there is limited research [23] on the impact of weave texture on the mechanical and shape memory properties of WFR-SMPCs, warranting further investigation.

To better understand the mechanisms by which woven structures influence the mechanical and shape memory properties of WFR-SMPCs, a systematic experimental study was conducted. Different mesostructured woven fabrics (plain, twill, and satin) were used to reinforce the SMP matrix using vacuum assisted resin infusion (VARI) process, and their effects on mechanical performance under different temperature conditions and loading scenarios were systematically tested. Macroscopic and microscopic observations were conducted on these WFR-SMPCs, and relevant structural parameters were measured. Uniaxial tensile tests were conducted on the SMP matrix at various temperatures to determine its mechanical properties and shape memory characteristics. Additionally, uniaxial tensile tests were performed on WFR-SMPCs

in both the (0/90°) and (±45°) directions under both fixed and programmable condition to evaluate the tensile and in-plane shear mechanical responses of the composites. The shape memory performance of the WFR-SMPCs was characterized through bending shape-recovery experiments. This allowed for a comparison of how different woven textures enhance the mechanical properties of SMPs and affect their shape memory capabilities. Understanding these effects is essential for optimizing material design and tailoring specific properties for various applications. For instance, enhanced mechanical properties and shape memory capabilities can significantly improve the functionality and reliability of deployable structures in aerospace engineering, biomedical devices, and smart wearable technologies. Moreover, this research provides mechanical property parameters and woven texture design experience for future investigations into more complex composite structures and multifunctional materials.

2. Materials and methods

2.1. Materials preparation

WFR-SMPCs are composed of a reinforcing phase and a matrix phase. In order to compare the effects of different woven textures on their mechanical and shape memory properties, the reinforcing phase employs three types of commercial woven fabrics with the same carbon fiber tows (AS4C-3 K, produced by HEXCEL Corporation) and similar surface densities but different woven textures: plain weave, twill weave, and satin weave. The fabrics are produced by Yixing Zhongfu Carbon Fiber Products Co., Ltd. The matrix phase uses an epoxy-based SMP resin developed by Leng's research group, which has a glass transition temperature (T_g) of 100 °C. The pure SMP resin specimens were prepared using molding method, while the WFR-SMPC specimens were made using the Vacuum Assisted Resin Infusion (VARI) process. The curing process was completed by a high-temperature drying oven (BPG-9200AH, manufactured by Shanghai Hengyi Technology Co., Ltd.), with a curing program set as a stepwise temperature increase of 80 °C/3h–100 °C/3h–150 °C/5h. The cutting dimensions and testing procedures of specimens refer to the testing standards of the American Society of Testing Materials (ASTM D638, D3039, D3518, and D6856).

2.2. Observation and calculation for materials

A digital optical microscope (VHX-900, produced by KEYENCE Corporation) was utilized to examine the micro-structure of the three types of WFR-SMPC specimens before and after testing. Detailed micro-geometric parameters in WFR-SMPCs, including the thickness of the tow, as well as the curvature radius and periodicity of the tow interlacing were observed. The fiber volume fraction V_f of WFR-SMPCs can be calculated by:

$$V_f = \left(1 - \frac{m_c - \sigma_f \times S}{\rho_m \times S \times t}\right) \times 100\% \quad (1)$$

where, m_c is the masses of WFR-SMPCs, σ_f is the areal density of woven fabrics, S is the area of WFR-SMPCs or the woven fabrics, ρ_m is the density of the SMP matrix, and t is the thickness of the WFR-SMPCs.

2.3. Uniaxial tensile tests for SMP and WFR-SMPCs

Uniaxial tensile tests on SMP and WFR-SMPCs at room temperature and high temperature were conducted using a universal testing machine

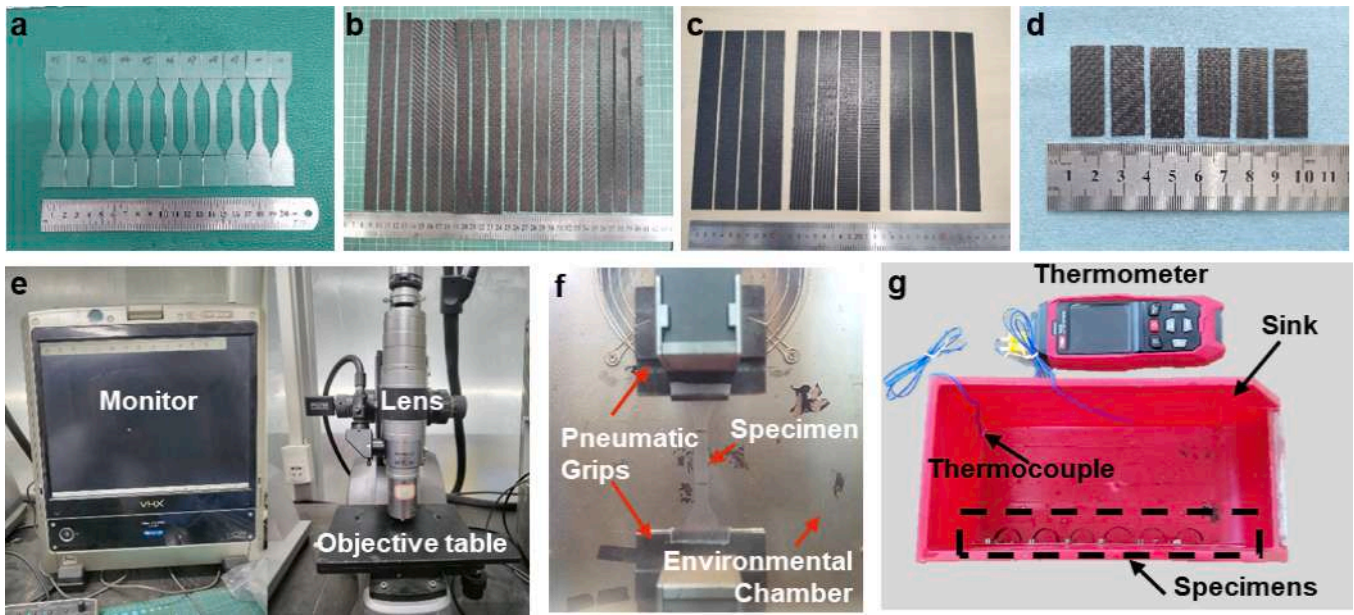


Fig. 1. Tested specimens and experimental equipment. (a) Pure epoxy-based shape memory polymer (SMP) specimens used for investigating the matrix properties of woven fabrics reinforced shape memory polymer composites (WFR-SMPCs); (b) to (d) Specimens used for analyzing the tensile, shear, and shape memory performance of WFR-SMPCs, respectively; (e) Optical microscope; (f) Universal testing machine; (g) Equipment for testing the shape memory performance of the WFR-SMPCs.

(Zwick/Roell Z010, load range: 10 kN, produced by Zwick Company), and an electronic universal testing machine with a temperature chamber (EUT4203, load range: 2 kN, manufactured by Shenzhen SAAS Testing Technology Co., Ltd).

- (1) For the characterization of pure SMP properties, the type IV dumbbell-shaped specimens specified in the ASTM D638 were selected for tensile testing, as shown in Fig. 1(a). The total length of the specimens is 115 mm, with a narrow section width of 6 mm and a thickness of about 3 mm. The initial distance between grips is 65 mm, and loading is controlled by a constant crosshead speed of 5 mm/min. Tensile tests with 1.5 % strain were performed at room temperature (20–40 °C), 5 % strain loading-recovery tests at moderate temperatures (60 and 80 °C), and 10 % strain loading-recovery tests at high temperatures (100 and 120 °C). This allowed us to obtain the tensile stress–strain response and shape memory recovery performance of SMPs at different temperatures.
- (2) For the tensile mechanical response of WFR-SMPCs in the fiber direction, uniaxial tensile tests at room temperature (25 °C) and high temperature (100 °C) were conducted on (0/90) single-layer laminae, referring to the ASTM D3039 and ASTM D6856 test standards. Three types of WFR-SMPCs were sampled from the 0-degree (warp) direction and the 90-degree (weft) direction, with a dimension of $230 \times 15 \times t$ mm, as shown in Fig. 1(b). The initial distance between grips is 150 mm, and the crosshead displacement speed is 2 mm/min. This enabled us to obtain the mechanical response of different WFR-SMPCs in the fiber direction at both room and high temperatures.
- (3) Regarding the in-plane shear mechanical response of WFR-SMPCs, uniaxial tensile tests at room temperature (25 °C) and high temperature (100 °C) were performed on (± 45) single-layer laminae, according to the ASTM D3518 and ASTM D6856 test standards, to induce an in-plane shear stress field. Three types of WFR-SMPCs were sampled from the +45-degree direction and the –45-degree direction, with a dimension of $230 \times 25 \times t$ mm, as shown in Fig. 1(c). The initial distance between grips is 150 mm, and the loading speed is 2 mm/min. This resulted in

obtaining the in-plane shear mechanical response of different WFR-SMPCs at room and high temperatures.

The shape memory fixity ratio R_{f-SMP} and recovery ratio R_{r-SMP} can be expressed as:

$$R_{f-SMP} = [1 - (\epsilon_0 - \epsilon_F)] \times 100\% \quad (2)$$

$$R_{r-SMP} = (1 - \epsilon_R) \times 100\% \quad (3)$$

where, ϵ_0 represents the strain of the deformed shape or the temporary shape, ϵ_F represents the strain in the fixed shape, ϵ_R represents the residual strain after shape memory recovery.

2.4. Shape memory performance test for WFR-SMPCs

To investigate the effects of different woven textures on the shape memory properties of WFR-SMPCs in different directions, specimens with (0/90) and (± 45) fiber directions from the three types of WFR-SMPCs (Fig. 1(d)) were selected to conduct bending-recovery tests for evaluating their shape memory performance. The dimensions of the specimens are: $35 \times 12.7 \times t$ mm. A schematic diagram of the shape memory property testing process is provided in Fig. 2(a). The material is heated to a temperature near its T_g to enable large deformation capability. With the aid of an external force and a mold, it can be shaped into a desired configuration (deformed shape). The external force is maintained until the material cools to room temperature, at which point the specimen is held in a temporary shape, having stored a small amount of elastic energy. After removing the external force, the stored elastic energy is released and the specimen retains a fixed shape. When reheated, the material can gradually return to its original shape. The shape memory performance of WFR-SMPCs can be determined by measuring the shape parameters at each stage, as depicted in Fig. 2(b). The shape recovery velocity V_r , shape fixity ratio R_f , and shape recovery ratio R_r can be calculated by:

$$V_r(t) = \frac{d\left(\frac{l}{r_2(t)}\right)}{dt} \quad (4)$$

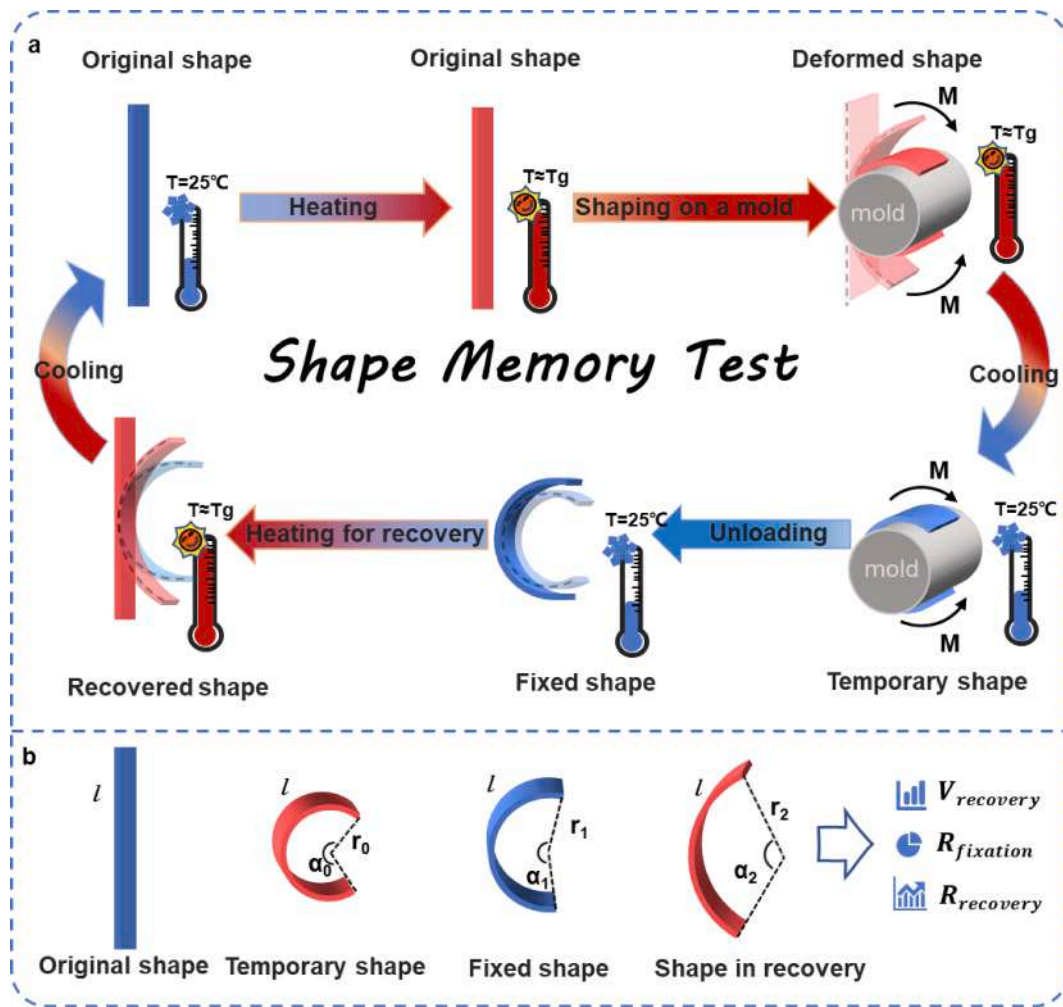


Fig. 2. Schematic diagram of the methodology for testing shape memory behavior and characterizing performance. (a) The shape memory test cycle; (b) Key parameters used in the calculation of shape memory performance.

$$R_f = \frac{r_0}{r_1} \times 100\% \quad (5)$$

$$R_r(t) = \left(1 - \frac{r_0}{r_2(t)}\right) \times 100\% \quad (6)$$

where, r_0 is the curvature radius of the temporary shape, r_1 is the curvature radius of the fixed shape, r_2 is the curvature radius during shape recovery process which varies with driving time t .

The deployment process was recorded with a camera during the experiment, and changes in the geometric dimensions of the specimens were measured during playback to characterize their recovery performance quantitatively. The drive temperature was recorded using a thermocouple thermometer (TA612C K-type, produced by Suzhou TASI Electronics Co., Ltd). The specific experimental steps are as follows: (1) Place the sample in a 120°C oven and maintain it for 20 min. (2) Use a metal bar with a diameter of 16 mm as the shaping mold, and bend it to fit onto the mold with an external force to obtain a temporary shape. (3) Maintain the external force until the material temperature decreases to room temperature to obtain a fixed shape. (4) Place the shaped specimens of different types in a sink, as shown in Fig. 1(g), then pour boiling water into the sink to simultaneously heat and drive the deployment of WFR-SMPCs.

3. Results and discussion

3.1. Optical morphology of woven fabrics and WFR-SMPCs

As illustrated in Fig. 3, plain, twill, and satin are three common types of woven structures, each with distinctive macro-morphological features. The plain weave is constructed by the interlacing of warp and weft tows over and under each other, resulting in a stable and uniform grid-like appearance, characterized by balance and homogeneity. The twill weave exhibits a staggered diagonal pattern created by longer floats of the tows, which gives the fabric a pronounced diagonal texture, offering greater compactness and directionality. The satin weave features even longer floats, with uneven distribution between warp and weft tows, leading to strong anisotropy. Table 1 presents the tow counts and relevant parameters for the three types of fabrics. The data indicates that, despite the similar areal density of the three fabrics, there are differences in tow densities and fabric thicknesses. These variations are attributed to the varying degrees of undulation in the tows, the spacing between them, and the differing interactions within the distinct woven textures.

As shown in Fig. 4, the three types of WFR-SMPCs all exhibit good quality, with the reinforcing materials closely integrated within the SMP matrix. The micro-morphology of the warp and weft tows can be observed from the z-x and z-y cross sections. Table 2 and Table 3 list the macro-parameters such as the thickness and fiber volume fraction of the WFR-SMPCs, as well as the micro-parameters including tow thickness, curvature radius, and undulation period length. The data from these

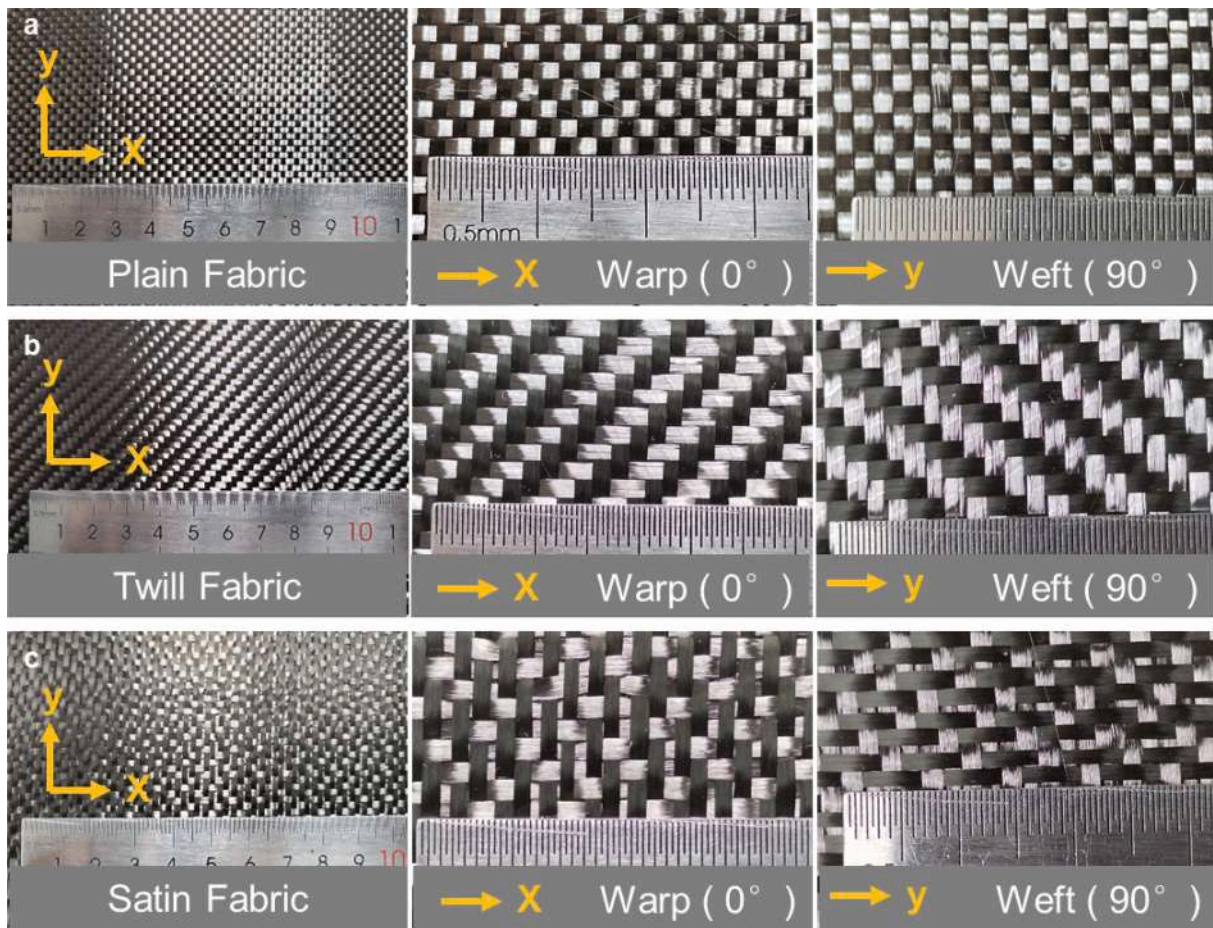


Fig. 3. Three types of woven fabrics with different woven textures. (a) Plain woven fabric; (b) Twill woven fabric; (c) Satin woven fabric.

Table 1

Macro parameters of the three kinds of woven fabrics.

Fabric Type	Fiber Type-Filament Count		Thread Count (Threads/ 10 cm)		Thickness (mm)	Areal Density (g/m ²)
	Warp	Weft	Warp	Weft		
Plain	AS4C-3	AS4C-3	55	52	0.236	220
Twill	K	K	57.5	60.5	0.225	220
Satin			57	53.5	0.225	225

tables reveal: (1) The fibers within the plain and twill tows are more uniformly dispersed, resulting in a consistent thickness of WFR-SMPCs. In contrast, the satin WFR-SMPC exhibits a greater thickness due to the fiber clustering within the satin tows, resulting in an increased tow thickness and, consequently, a thicker composite overall. (2) The fiber volume fractions of the plain and twill WFR-SMPCs are similar, both exceeding 60 %. However, the satin WFR-SMPC has a fiber volume fraction below 60 %, as its larger thickness accommodates more resin, thus reducing the fraction of fibers. (3) The tows within the plain WFR-SMPC exhibit a small curvature radius and a short weave period. In the twill WFR-SMPC, the tows have a larger radius of curvature, with the frequency of undulation changes being half that of the plain WFR-SMPC. The satin WFR-SMPC features tows that alternate between large and small radii of curvature, similar to the twill's undulation frequency. These tow differences are anticipated to affect the stiffness and deformability of WFR-SMPCs, which will be investigated further through uniaxial tensile tests.

3.2. Performance characterization of SMP matrix

Fig. 5(a) illustrates the tensile mechanical response of the SMP matrix at various temperatures (20–120 °C) and its shape memory recovery performance at high temperatures (60–120 °C). Fig. 5(b) depicts the trend of the tangent modulus at 0.2 % strain, the secant modulus within the 0–1.5 % strain range, and the shape recovery ratio with respect to temperature. As the temperature increases, there is a notable change in the mechanical behavior of the SMP; it exhibits excellent mechanical properties at room temperature with an elastic modulus greater than 2 GPa, indicating good load-bearing capacity. Beyond 40 °C, the elastic modulus sharply declines, suggesting a reduction in material stiffness and an enhancement in deformability. At 100 °C, the elastic modulus falls below 40 MPa, a decrease by two orders of magnitude, endowing the material with superior deformability. The shape memory recovery performance of the SMP improves with increasing temperature within the 60–120 °C range. Above 100 °C, it achieves a shape recovery ratio of over 99 %, and the mechanical response during the tensile-recovery test at a large strain of 10 % demonstrates a linear relationship.

3.3. Tensile response of different (0/90) WFR-SMPCs

3.3.1. Tensile properties of WFR-SMPCs

The tensile mechanical responses test results (Fig. 6) for (0/90) WFR-SMPCs show that at both room and high temperatures, the fabric significantly reinforces the mechanical properties of the WFR-SMPCs in the fiber direction, yet the matrix's large deformability is considerably restricted. At room temperature, the stress-strain relationship of the (0/90) WFR-SMPCs exhibits a linear behavior; whereas at high temperature, it starts with a nonlinear stress-strain relation, followed by a linear

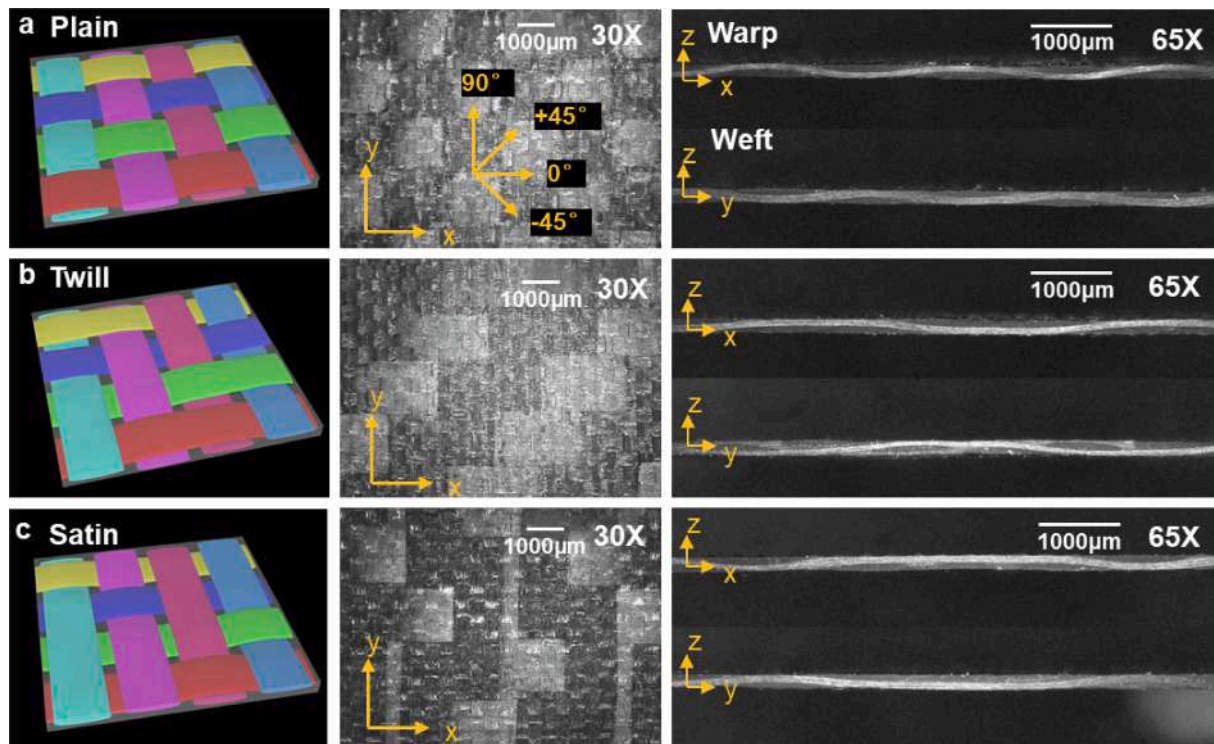


Fig. 4. Microscopic characterization of WFR-SMPCs reinforced with different woven fabrics. (a) Plain woven fabric reinforced WFR-SMPCs; (b) Twill woven fabric reinforced WFR-SMPCs; (c) Satin woven fabric reinforced WFR-SMPCs.

Table 2
Parameters of WFR-SMPCs reinforced with different woven fabrics.

Type	Thickness (mm)	Density (g/cm ³)		Fiber Volume Fraction(%)
		SMP Matrix	WFR-SMPCs	
Plain-WFR-SMPC	0.341 ± 0.008	1.21	1.46 ± 0.02	62.81 ± 1.37
Twill-WFR-SMPC	0.354 ± 0.020		1.45 ± 0.09	61.68 ± 5.15
Satin-WFR-SMPC	0.356 ± 0.019		1.52 ± 0.03	57.94 ± 1.12

Table 3
Parameters of tows in different WFR-SMPCs.

Type	Thickness (mm)		Curvature Radius (mm)		Undulation Period (mm)	
	Warp	Weft	Warp	Weft	Warp	Weft
Plain	0.109	0.125	4.841	5.684	3.774	3.706
Twill	0.123	0.100	16.139	15.010	6.748	6.634
Satin	0.143	0.167	5.226/ 35.629	5.120/ 29.645	7.352	6.824

pattern. In room temperature, WFR-SMPCs demonstrate superior load-bearing capacity and elongation at break compared to those at higher temperature. This is attributed to the SMP matrix effectively binding the woven fabric at room temperature, which facilitates the dispersion and transfer of loads, whereas at high temperature, the matrix's mechanical properties and the interfacial performance between the fibers and the matrix are weaker, and the mechanical properties of the carbon fibers also degrade under high-temperature conditions.

The curvature radius and undulation period of the tows in different fabrics have a significant impact on the tensile mechanical response and deformability of the WFR-SMPCs. At both room temperature and elevated temperature, the modulus values of the three WFR-SMPCs

indicate that satin-weave composite possesses the highest modulus, followed by twill-weave and plain-weave composites. Moreover, the length of the initial nonlinear deformation at high temperature also follows this hierarchical order. This variation is due to the differing undulation patterns of the tows in the woven textures. As indicated in Table 3, the tows of plain weave have the smallest average curvature radius and periodicity, which results in lower modulus for the WFR-SMPC. Similarly, in the satin WFR-SMPC, the tows have larger average curvature radius and longer periodicity, exhibiting a higher modulus and shorter nonlinear stage at high temperature. The tow curvature and periodicity of twill WFR-SMPC fall between the other two types.

In addition, for the three types of WFR-SMPCs, there is a discernible difference in the tensile modulus between the 0° direction (warp direction) and the 90° direction (weft direction). The characteristics of tow undulation mentioned earlier are the primary reason; the direction with less tow curvature and longer periodicity tends to have a higher modulus and less deformability. Conversely, it will exhibit lower modulus and greater deformability. While the influence of the difference in the number of tows in the two directions, as shown in Table 1, is comparatively small.

3.3.2. Tensile failure mode analysis of WFR-SMPC

Fig. 7 compares the fracture morphology of different (0/90) WFR-SMPCs after uniaxial tensile testing at room and high temperatures. At room temperature, the specimens exhibit multiple fracture sites with brittle failure of longitudinal fibers and ordered transverse fibers. While the specimens at high temperature show a singular fracture site with brittle failure of longitudinal fibers accompanied by detachment of the transverse fibers. This is due to the SMP matrix's glassy state at room temperature, which has higher modulus and strength, exerting greater constraint on the fibers. At room temperature, the rapid release of energy upon breaking creates stress waves that induce multiple fracture sites in the material. While at high temperature, the SMP matrix in a viscoelastic state, with lower modulus and strength as well as high damping, allows for energy dissipation and reducing constraint to the

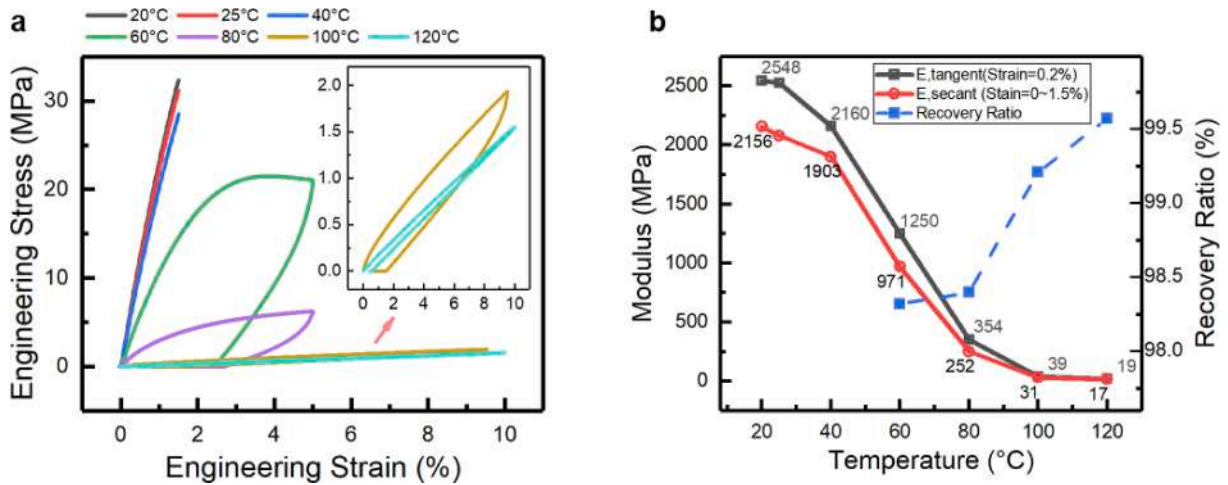


Fig. 5. Tensile mechanical properties and shape memory performance of SMP. (a) Stress–strain curves of SMP at different temperatures; (b) Curves of Young’s modulus and recovery ratio of SMP with temperature.

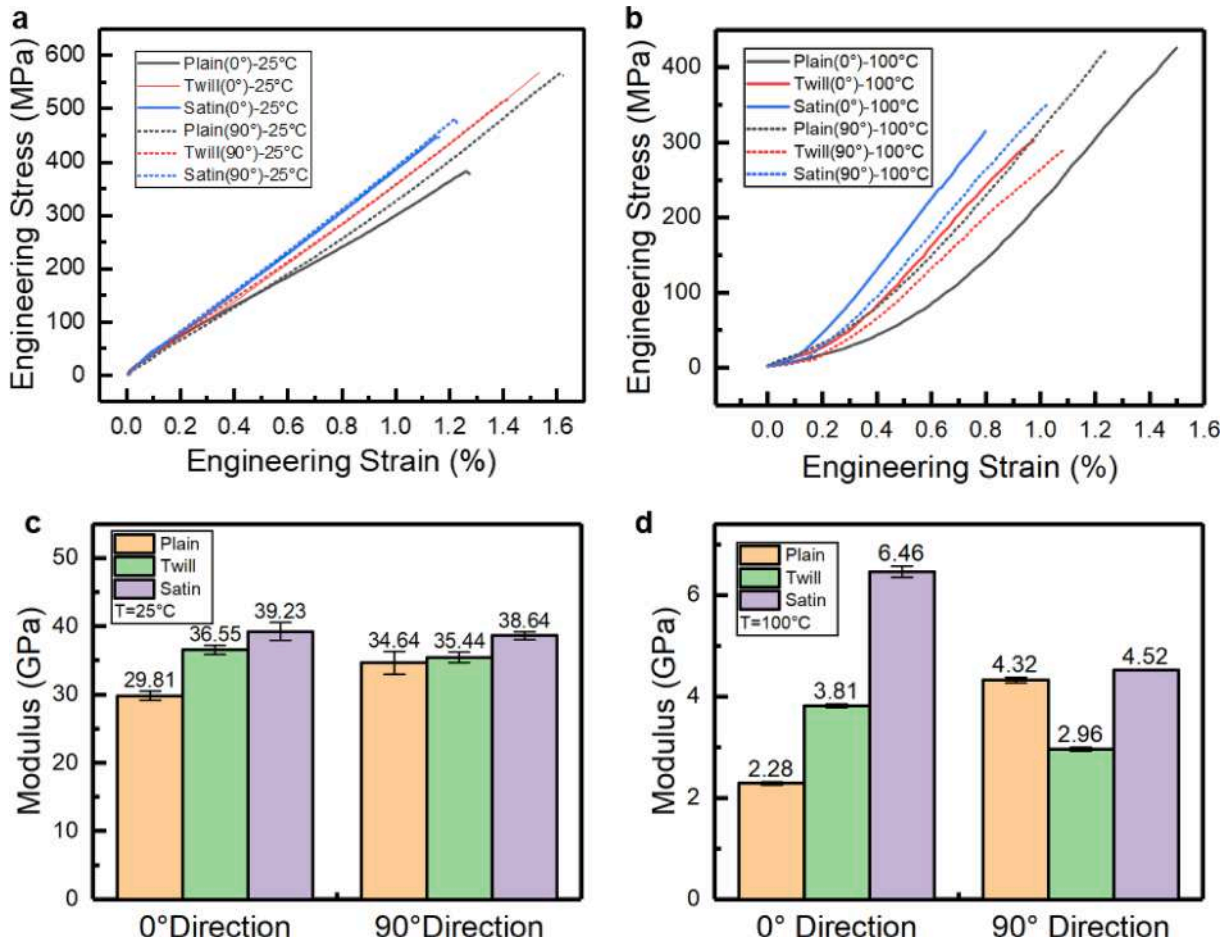


Fig. 6. Tensile test results for (0/90) WFR-SMPCs reinforced with different woven fabrics in the warp (0°) and weft (90°) directions, tested at 25 °C and 100 °C. (a) and (b) Stress–strain curves of WFR-SMPCs at 25 °C and 100 °C; (c) and (d) Comparison of Young’s moduli of WFR-SMPCs at 25 °C and 100 °C.

fibers leading to singular fracture and transverse fiber detachment.

3.4. In-plane shear response of different (± 45) WFR-SMPCs

3.4.1. In-plane shear properties of WFR-SMPCs

Fig. 8(a)–(c) and (d)–(f) display the tensile force–displacement curves of different WFR-SMPCs at $+45^\circ$ and -45° directions under 25 °C

and 100 °C, respectively. Fig. 8(g)–(i) and (j)–(l) summarize the displacements of linear region, failure displacements, maximum loads of linear region, peak loads, work in the linear region, and the total work of different WFR-SMPCs at 25 °C and 100 °C, respectively. The results indicate that:

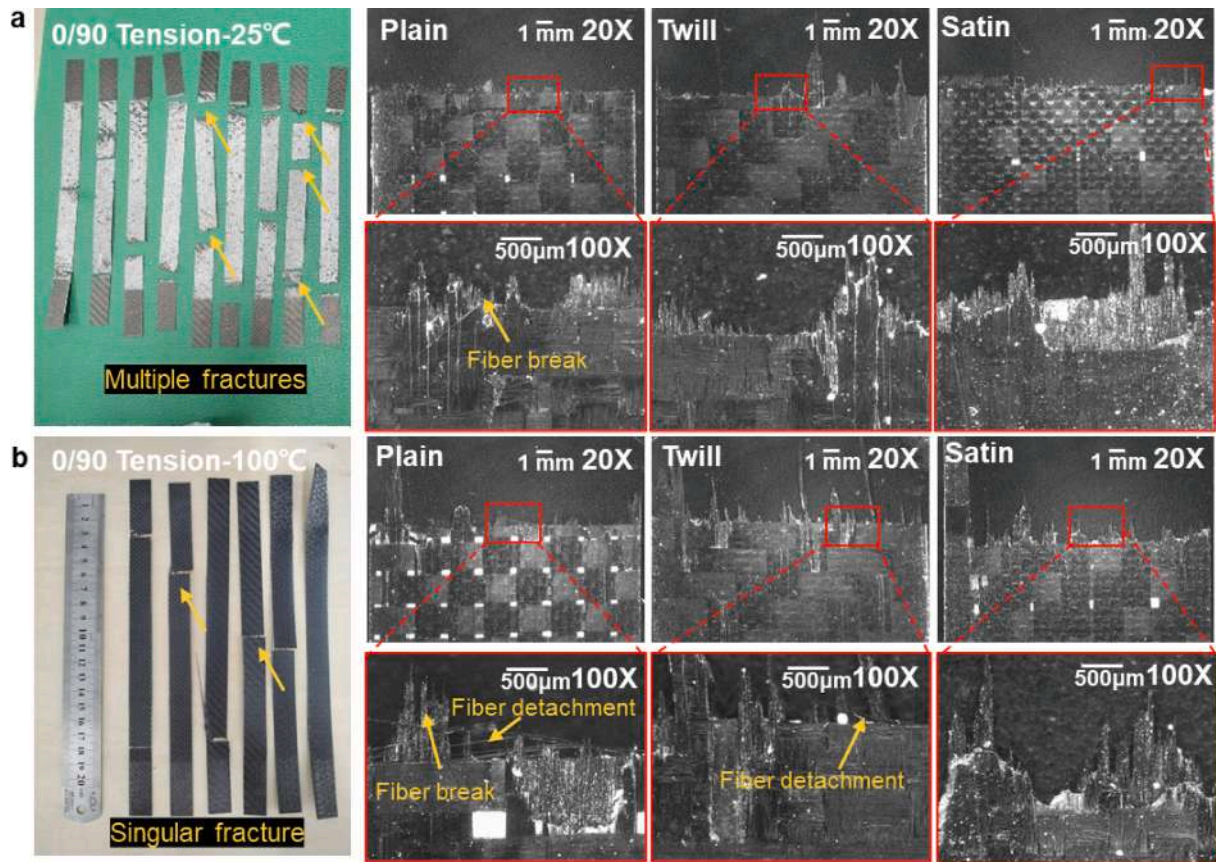


Fig. 7. Tensile fracture morphology of (0/90) WFR-SMPCs reinforced with different woven fabrics at (a) 25 °C and (b) 100 °C.

- (1) Force-displacement response: Initially, the three types of WFR-SMPCs exhibit similar mechanical responses at both room and high temperatures, yet display significant differences in the nonlinear region. This is due to different interactions between tows in different woven textures caused by larger deformations.
- (2) Mechanical properties at $+45^\circ$ and -45° directions: Plain WFR-SMPCs demonstrate higher consistency at both low and high temperatures, owing to the high degree of uniformity in both directions. Twill WFR-SMPCs show variability at both temperatures due to the anisotropy of the twill fabric texture, especially at high temperature. Satin WFR-SMPCs exhibit greater variability at low temperature but higher consistency at high temperature. This is because the anisotropy of looser satin woven texture is protected by the matrix at low temperatures, whereas at high temperatures, the constraining effect of matrix diminishes, preventing expression of the texture's anisotropy.
- (3) Deformation and load capacity in the linear stage: The linear displacements of the three WFR-SMPCs have similar values. The average linear deformation at high temperature is about 3.4 times that of room temperature, while the average load capacities at high temperature reduce to one third of that at room temperature.
- (4) Maximum displacement and load capacity: Due to its tight weave structure, plain WFR-SMPC possesses the highest failure displacement and load capacity, showing consistency in both $\pm 45^\circ$ directions. In contrast, twill and satin WFR-SMPCs have lower maximum displacements and load capacities compared to plain WFR-SMPC, and have relatively large differences in $\pm 45^\circ$ directions. This is due to their looser interlacing structures and anisotropic textures.
- (5) Energy absorption: The plain WFR-SMPC has greater interlacing amplitude and frequency of the tows, which can withstand larger

deformations without failure, thus exhibiting excellent energy absorption capabilities under tension. At room temperature, due to strong matrix constraints, the same type of WFR-SMPCs shows little difference in energy absorption between the $\pm 45^\circ$ directions. However, high temperature increases disparity, notably in twill WFR-SMPC caused by asymmetry and anisotropy between the two directions.

The shear stress-strain curves for the WFR-SMPCs in the $+45^\circ$ and -45° directions under room temperature and high temperature are shown in Fig. 9(a) and (b). It is evident that the mechanical responses of WFR-SMPCs with the same texture have good repeatability in the same direction, but there are differences in different textures or directions: (1) At room temperature, the satin WFR-SMPCs show the best mechanical performance in the $+45^\circ$ direction, but the worst in the -45° direction. The properties of twill WFR-SMPCs are slightly better than that of the plain WFR-SMPCs. The response of plain and twill WFR-SMPCs exhibit negligible difference in the two directions, while the satin WFR-SMPCs show a significant difference. (2) At high temperature, the mechanical performance of twill WFR-SMPCs, especially in the -45° is the best, followed by the plain and satin WFR-SMPCs. The plain WFR-SMPCs show the smallest difference in mechanical response between the two directions.

Due to the significant nonlinearity of the shear stress-strain curves, the shear modulus G_{12} is taken as the tangent shear modulus at 0.5 % and 10 % strain, respectively. Fig. 9(c) and (d) summarize the shear modulus of different WFR-SMPCs at small shear strain (0.5 %) and large shear strain (10 %) under room temperature and high temperature, respectively. Under small shear strain, the shear moduli of the plain, twill, and satin WFR-SMPCs at room temperature are 13.56, 13.69, and 20.35 times that of their values at high temperature, while under large shear strain, they are 1.94, 1.98, and 2.02 times, respectively. This

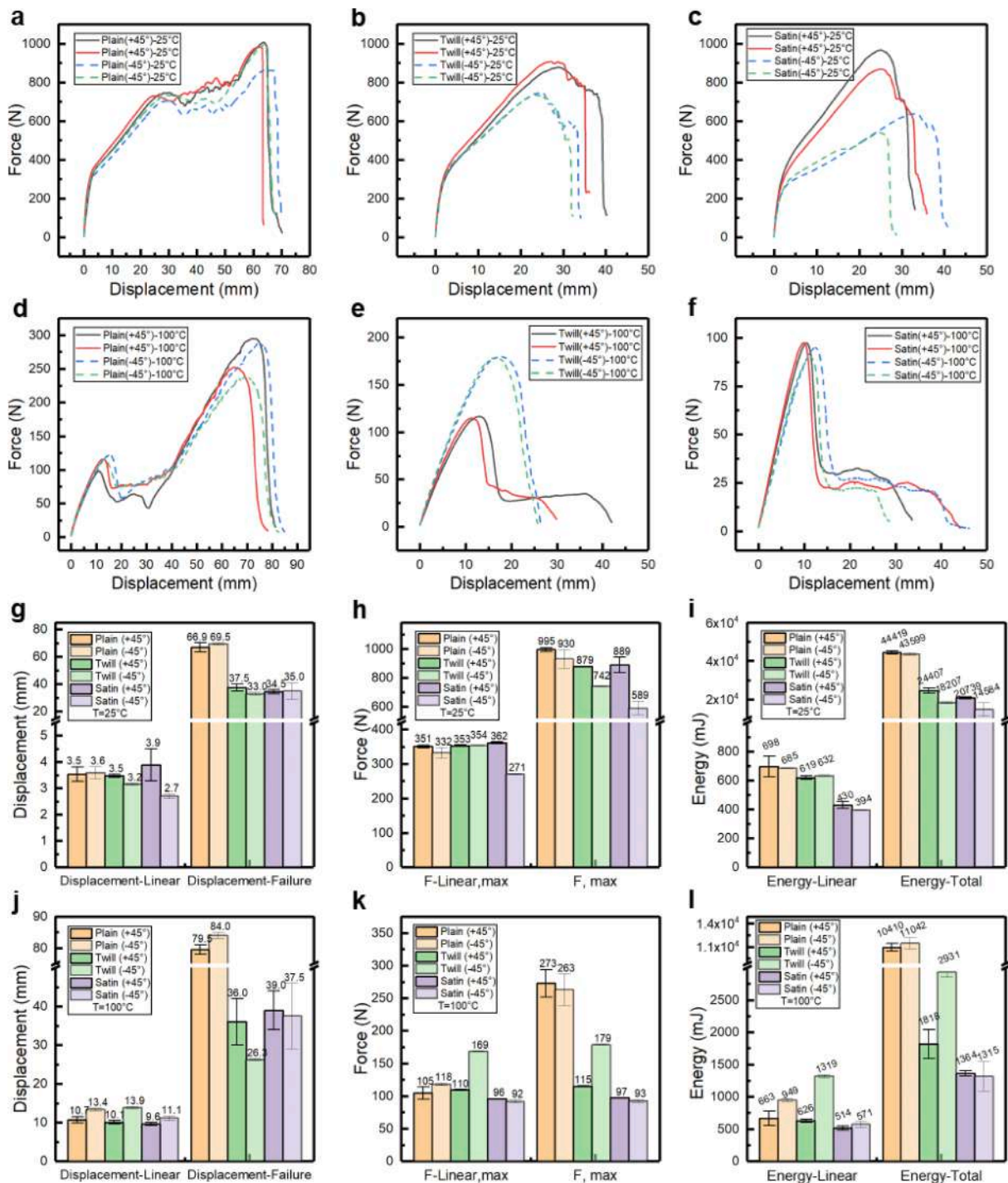


Fig. 8. Mechanical response of (±45) WFR-SMPCs reinforced with different woven fabrics under uniaxial tension at 25 °C and 100 °C. (a) to (c) Force-displacement curves at 25 °C; (d) to (f) Force-displacement curves at 100 °C; (g) to (i) Displacement, force, and energy dissipation at 25 °C; (j) to (l) Displacement, force, and energy dissipation at 100 °C.

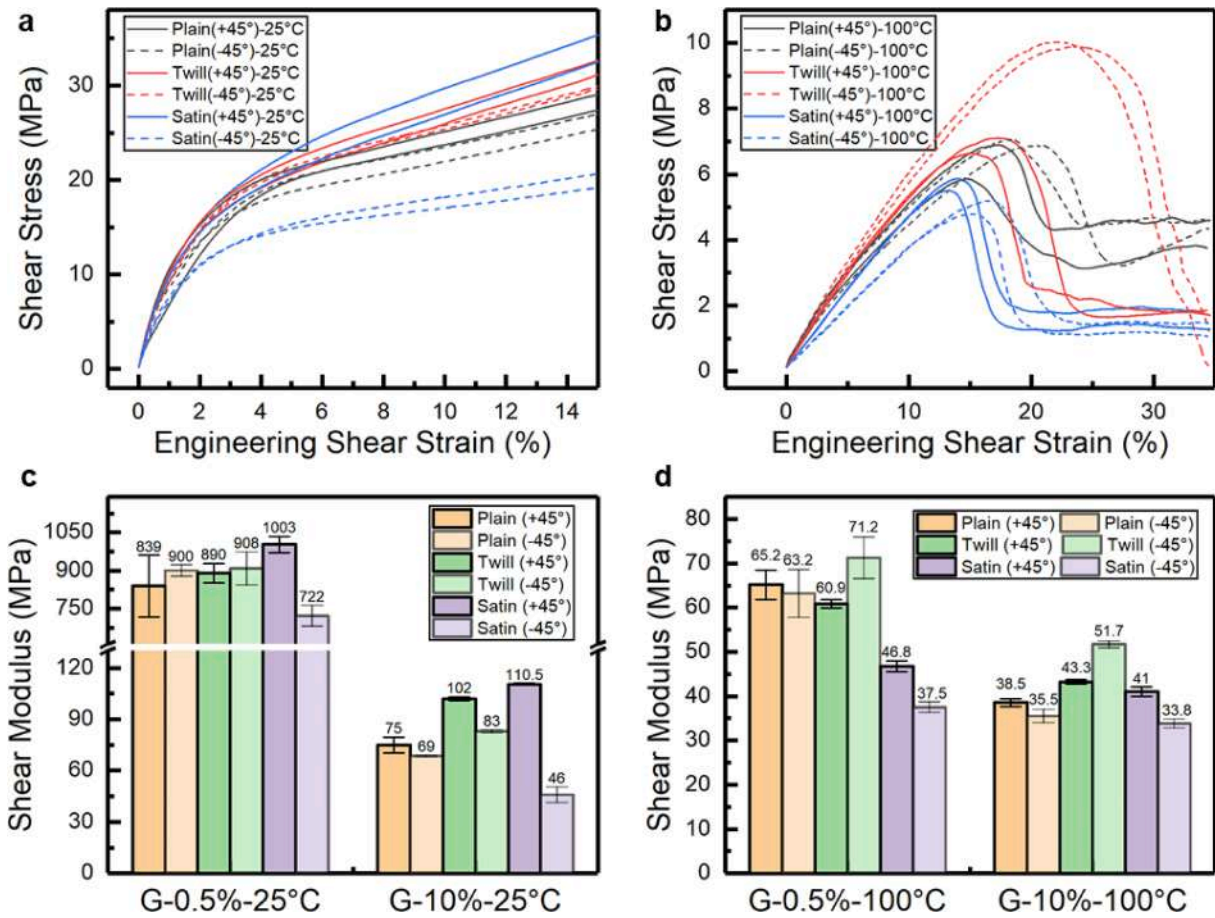


Fig. 9. In-plane shear properties of (±45) WFR-SMPCs with different woven fabrics under uniaxial tension at 25 °C and 100 °C. (a) to (b) Shear stress-shear strain curves at 25 °C and 100 °C; (c) to (d) Comparison of shear moduli at 25 °C and 100 °C.

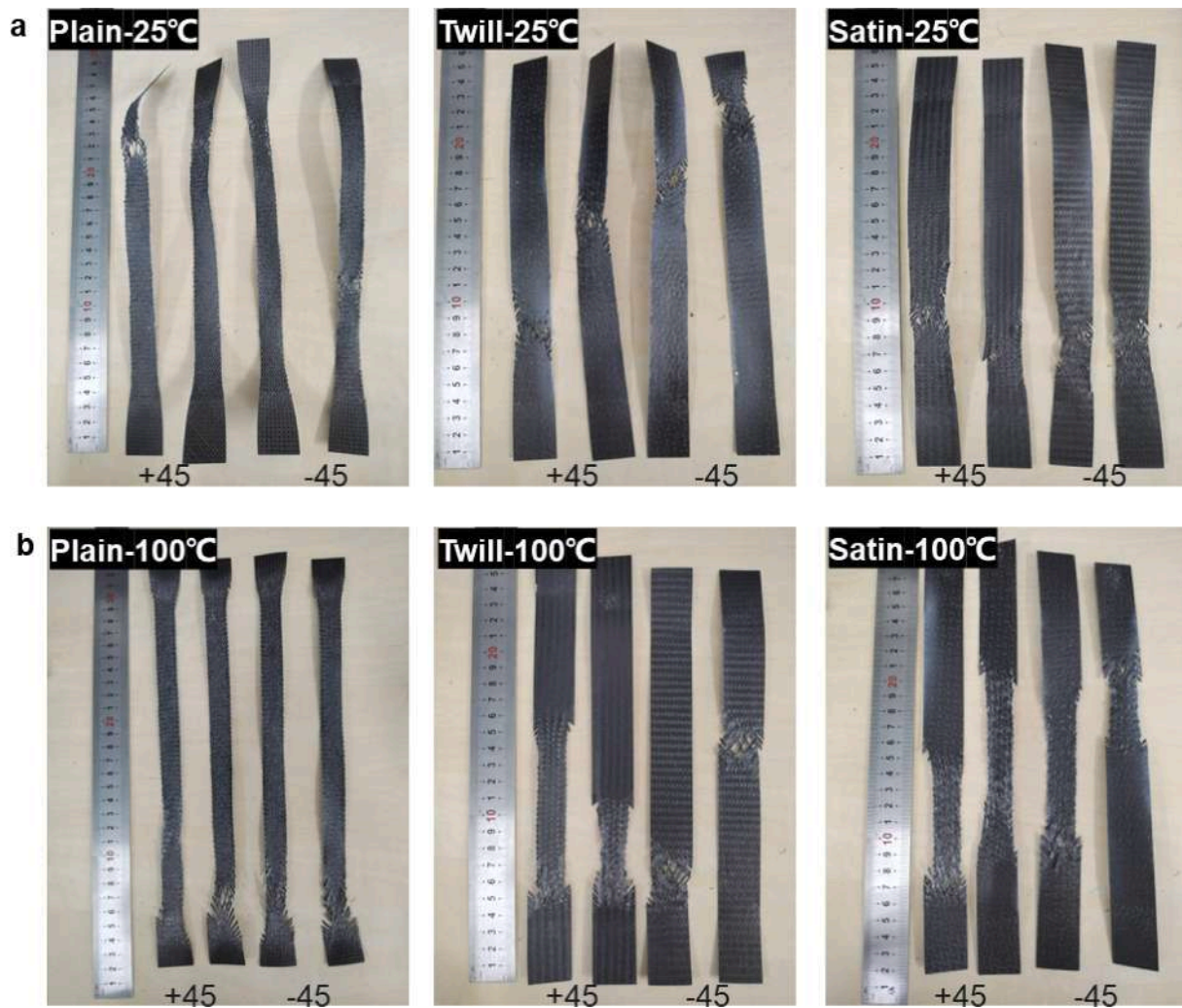


Fig. 10. Comparison of (± 45) WFR-SMPCs with different woven fabrics after uniaxial tensile testing at (a) 25 °C and (b) 100 °C.

suggests that the shear modulus of WFR-SMPCs is affected by temperature differently depending on the level of shear strain: (1) Under small shear strain, the shear performance of WFR-SMPCs is highly sensitive to temperature, where the influence of temperature on the SMP matrix plays a dominant role. (2) Under large shear strain, the sensitivity of the shear performance of WFR-SMPCs to temperature is relatively smaller, indicating that the woven texture plays a more significant role. (3) Under both small and large shear strains, temperature has a greater influence on the shear performance of satin WFR-SMPCs than on the twill and plain ones. This is due to the looser interaction between the tows in the satin WFR-SMPCs.

3.4.2. In-plane shear failure mode analysis of WFR-SMPC

From the macroscopic images after in-plane shear tensile testing (Fig. 10), it can be found that: (1) For plain WFR-SMPCs, local necking caused by shear at both room and high temperatures extends throughout the entire specimen leading to failure. (2) For twill WFR-SMPCs, only the +45° direction specimens exhibit an extension of local necking in high-temperature tensile tests, while other specimens are locally damaged subjected to the shear load. (3) Satin WFR-SMPCs demonstrate local shear failure at room temperature, whereas at high temperatures, local shear extends a certain distance before failure occurs.

Examining the microscopic images of shear failure for the three types of WFR-SMPCs in Fig. 11 reveals: (1) At room temperature, the stiff SMP matrix causes inter-fiber crushing in fiber bundles across all three types of WFR-SMPCs. Plain weave's tight interlacing causes shear-induced

matrix failure; twill exhibits fiber breakages at the fracture site; satin has a looser structure with some tow twisting. (2) At high temperatures, the flexible SMP matrix prevents fiber bundle crushing, with primary damage from tow rotation under shear, causing matrix failure and detachment of tows.

3.5. Shape memory performance of different WFR-SMPCs

Fig. 12(a) and (b) illustrate the fixed shapes of the three types of WFR-SMPCs in the (0/90) and (± 45) directions after shaping, along with their comparisons. The radius of curvature for each specimen in the fixed shape was measured, and the shape fixity ratio R_f could be calculated using Eq. (5). The fixity ratios for these WFR-SMPCs are shown in Fig. 13(a), from which it can be observed that (1) for the fiber orientation, the shape fixity ratio of the three WFR-SMPCs is higher in the (0/90) direction than that in the (± 45) direction, and (2) regarding the woven texture, the satin WFR-SMPCs exhibit the highest shape fixity ratio in both directions, followed by twill and plain WFR-SMPCs.

Fig. 12(c) demonstrates the deployment process of different WFR-SMPCs in hot water. During the first 15 s of the deployment process, the temperature is maintained above 86 °C, then gradually decreases to 79 °C. The radius of curvature for each specimen at various time points during the deployment was measured, and the angular velocity V_r and shape recovery ratio R_r of the specimen over time could be calculated using Eqs. (4) and (6). As shown in Fig. 13(b), (c), and (d), after 2.5 s, the central angles of the specimens rapidly decrease, indicating a rapid

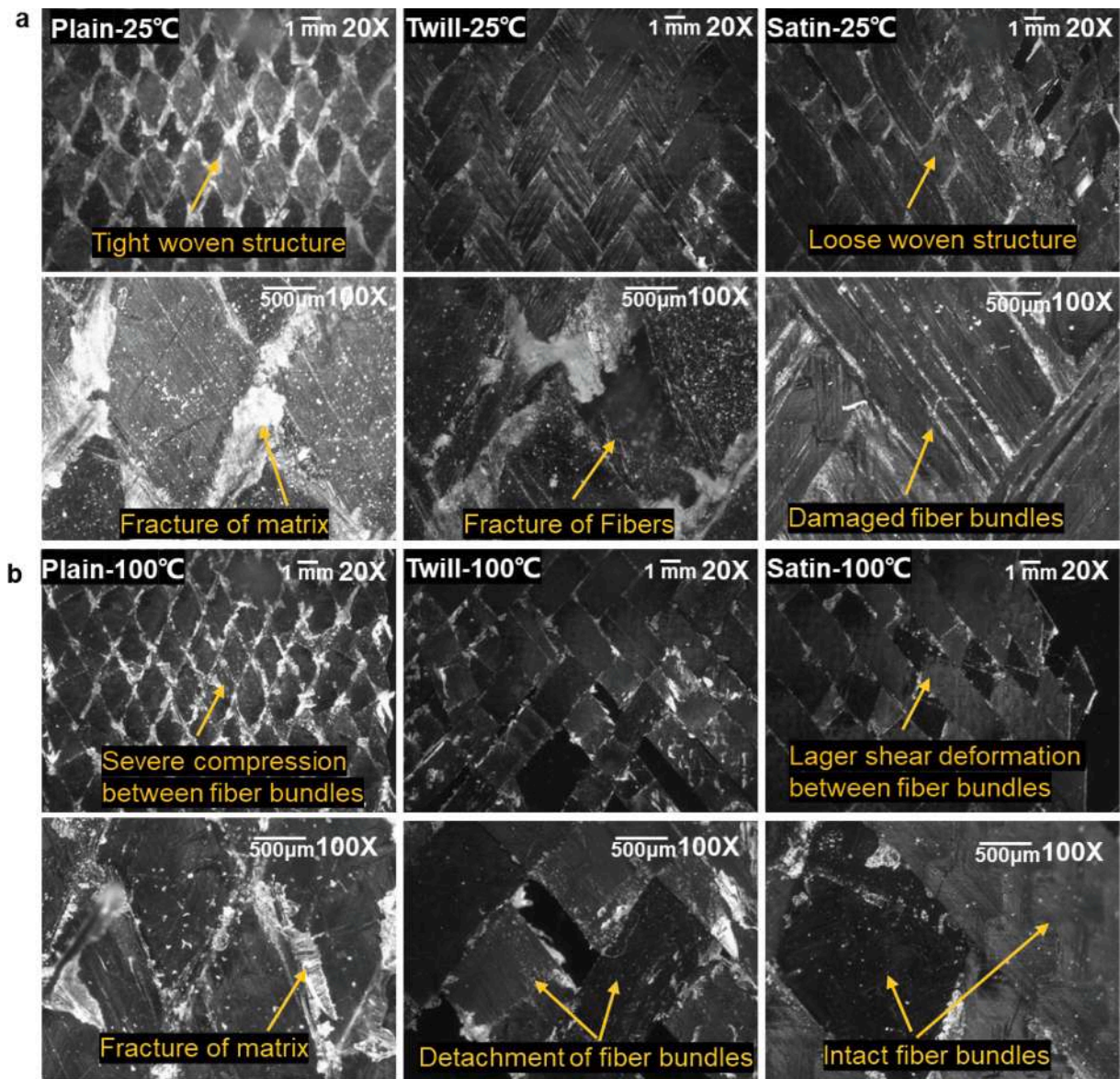


Fig. 11. In-plane shear fracture morphology of (± 45) WFR-SMPCs reinforced with different woven fabrics at (a) 25 °C and (b) 100 °C.

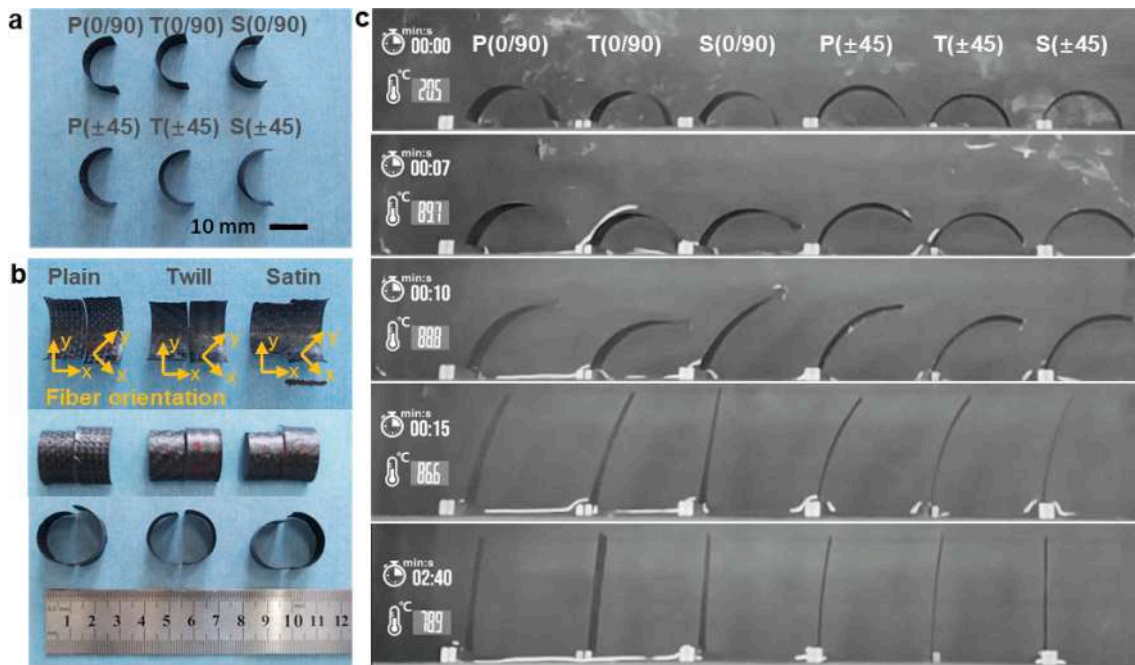


Fig. 12. Characterization of shape memory performance for WFR-SMPCs with different woven fabrics in (0/90) and (±45) directions. (a) Fixed shape of WFR-SMPC specimens; (b) Comparison of fixed shapes from the front, back, and side; (c) Deployment process of tested specimens. Note: In the figures, the letters P, T, and S represent the woven texture of the specimens as plain, twill, and satin, respectively.

increase in the unfolding speed. Around 10 s, the unfolding speed peaks and then gradually reduces. Between 2.5 and 20 s, the average unfolding speed of all specimens reaches $10^\circ/\text{s}$, with the maximum peak speed at $28^\circ/\text{s}$ and the minimum at $17^\circ/\text{s}$. During the unfolding process, the (0/90) satin WFR-SMPC recovers the fastest, while the (±45) plain WFR-SMPC is the slowest. By 20 s, all specimens are essentially flat, with each achieving a recovery ratio of over 80 %, and by 160 s, the recovery ratio exceeds 93 %. The satin WFR-SMPCs show the highest recovery ratios, reaching over 99.6 % in both directions. Twill WFR-SMPCs follow, with a recovery ratio of 99.1 % in the (0/90) direction and 96.1 % in the (±45) direction. Plain WFR-SMPCs show a significant difference between the two directions, with a recovery ratio of 98.6 % in the (0/90) direction and a relatively lower value of 93.2 % in the (±45) direction.

From the micro-morphology of the shaped WFR-SMPCs, it is evident that: (1) In the (0/90) specimens, as shown in Fig. 14(a)–(c), local wrinkling is most pronounced in plain and twill WFR-SMPCs compared to satin. This wrinkling occurs where longitudinal and transverse tows interlace, causing microscopic fiber buckling characteristics. Plain and satin weaves exhibit short C-shaped fiber buckles due to shorter floating spans, while twill weave displays long S-shaped buckles from longer spans and less interlacing. (2) In the (±45) specimens, as shown in Fig. 14(d)–(f), the bending deformation is uniformly smooth on the inner surface of the specimen, with only small shear occurring between tows. Among these samples, satin WFR-SMPC shows the largest shear angle of the tows, followed by twill, with plain having the smallest shear angle.

Combining the previously calculated fiber volume fraction and shape memory performance analysis of different WFR-SMPCs, it can be understood that: (1) In the (0/90) direction, satin and twill WFR-SMPCs have higher matrix fraction and smoother local wrinkles, and the fiber orientation is along the bending direction, resulting in higher fixity ratios, recovery speeds, and recovery ratios. In contrast, plain weave, with lower matrix fraction and more acute local wrinkling, suffers greater damage, leading to inferior shape memory properties. (2) For (±45) WFR-SMPCs, the shear deformation between tows presents certain resistance to shape recovery, making their shape memory properties

inferior to those in the (0/90) direction. Especially for plain and twill ones, tight interlacing intensifies the impact of shear deformation after bending, further reducing the recovery ratios. The looser interlacing of the satin weave facilitates the material's shape recovery.

4. Conclusions

This study analyzed the reinforcing effects of different woven textures on SMP, providing experimental data on microstructure, mechanical properties, and shape memory behavior. The results revealed:

- All woven fabrics enhanced SMP's mechanical properties, with variations in deformability and enhancement directionally dependent on the fiber orientation.
- The anisotropic mechanical properties induced by woven textures differentially governed WFR-SMPCs' in-plane shear performance in fixed and programmable states. The satin-weave WFR-SMPC exhibited the highest shear modulus of 1003 MPa in the fixed state (25 °C), whereas the twill-weave variant demonstrated a maximum shear modulus of 71.2 MPa in the programmable state (100 °C).
- Regarding shape memory performance, all WFR-SMPCs exhibited higher shape fixity ratio, recovery ratio, and recovery speed when tested in the (0/90) direction compared to the (±45) direction. This is attributed to the more effective reinforcement of (0/90) fiber orientations, whereas (±45) orientations undergo shear deformation during bending.
- The satin-weave WFR-SMPC demonstrated the best shape memory performance with a shape fixity ratio greater than 78.1 % and a shape recovery ratio over 99.6 %, followed by twill and plain, influenced by tow interlacing and resin fraction.
- Microscopic analysis during bending showed local wrinkles in (0/90) specimens and inter-tow shear slippage in (±45) specimens, with variations among weave types affecting shape memory characteristics.

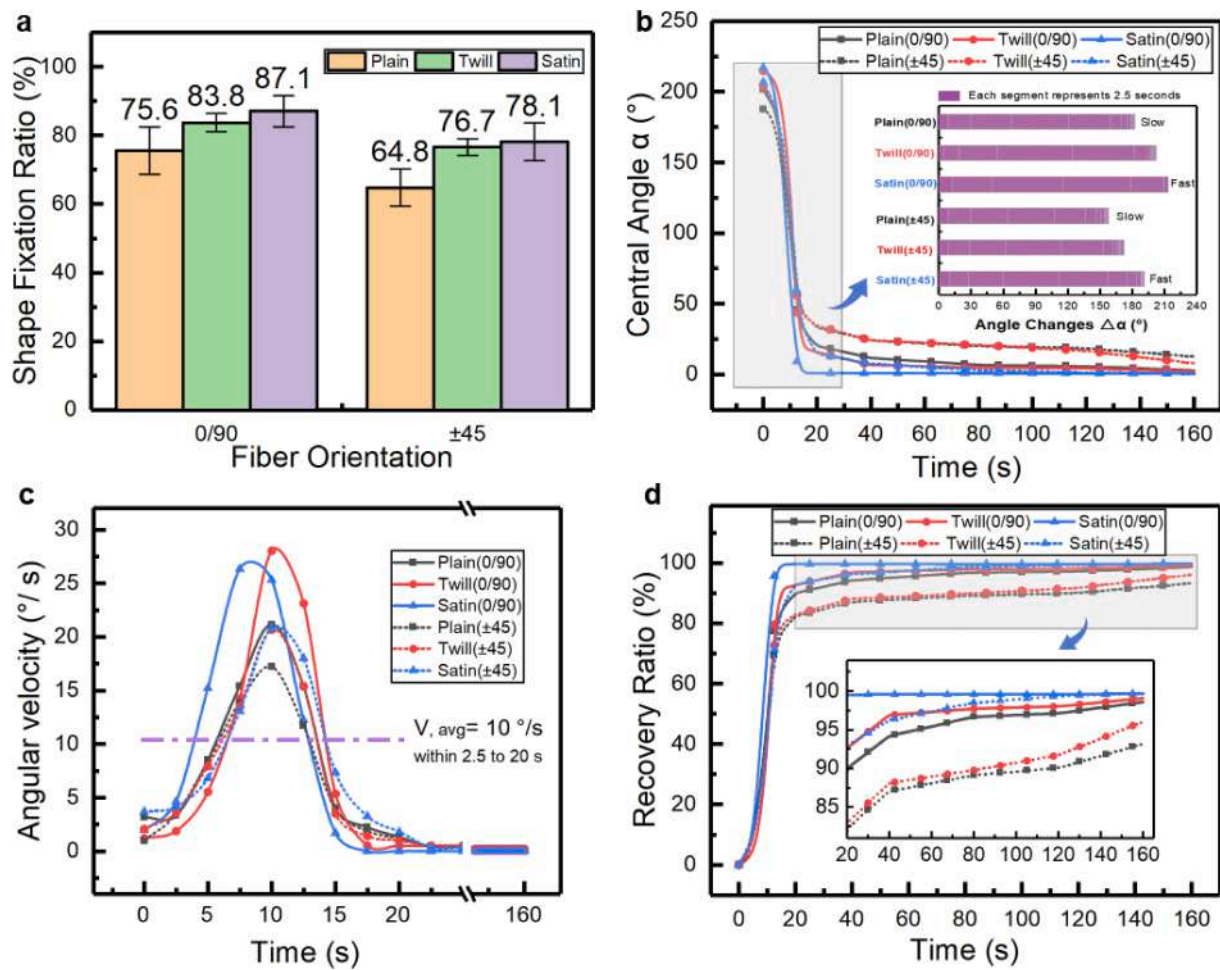


Fig. 13. Results of shape memory performance tests for WFR-SMPCs with different reinforced fabrics in (0/90) and (±45) directions. (a) Shape fixity ratio of tested WFR-SMPCs; (b) The curves of the central angle of WFR-SMPCs over time; (c) The curves of the angular velocity of WFR-SMPCs over time; (d) The curves of the recovery ratio of WFR-SMPCs over time.

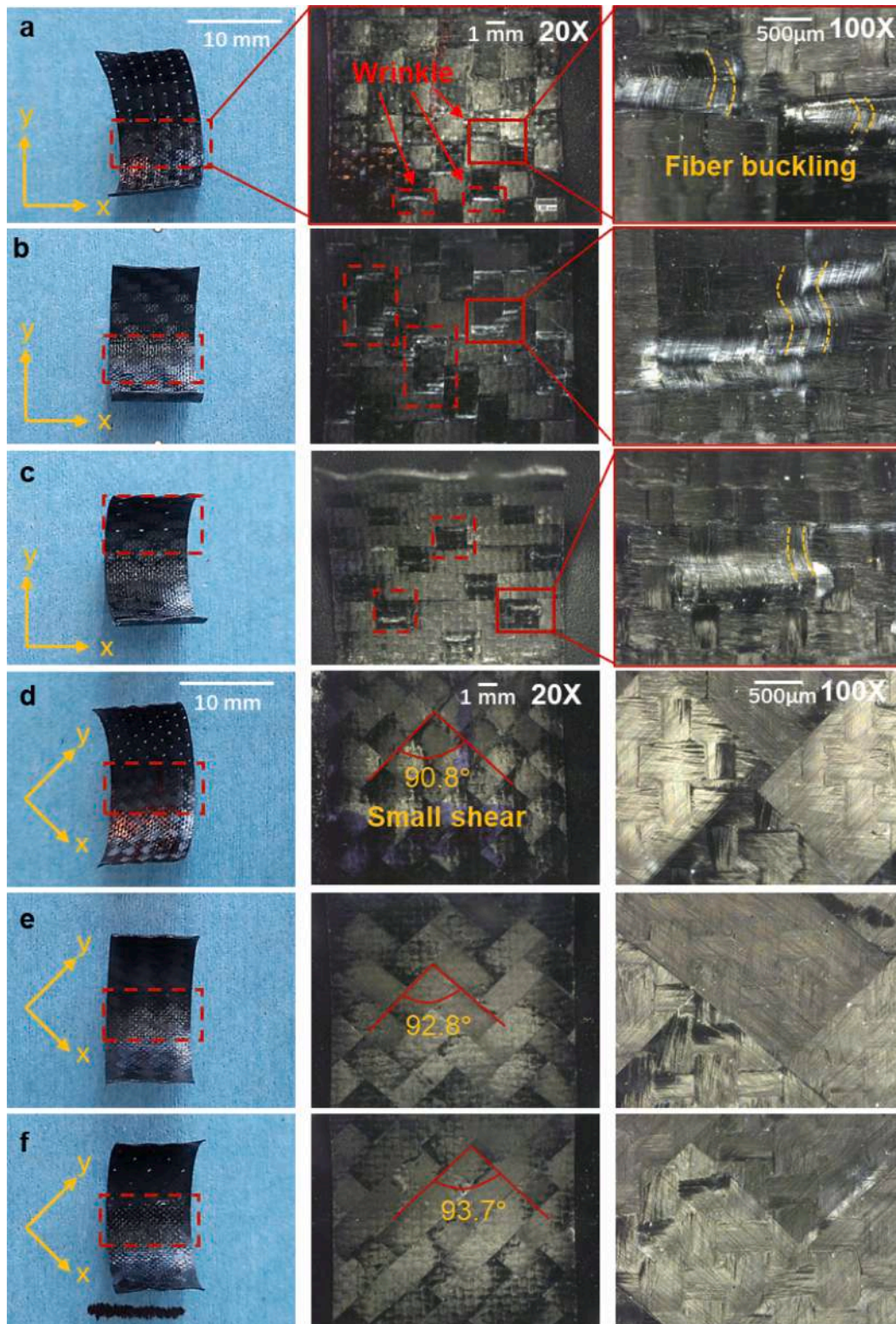


Fig. 14. Morphology analysis of shaped WFR-SMPCs with different reinforced fabrics in (0/90) and (± 45) directions. (a) to (c) (0/90) WFR-SMPCs with plain, twill and satin woven fabrics, respectively; (d) to (f) (± 45) WFR-SMPCs with plain, twill and satin woven fabrics, respectively.

CRediT authorship contribution statement

Guangqing Ming: Writing – review & editing, Writing – original draft, Visualization, Methodology, Investigation, Conceptualization. **Mingming Xu:** Writing – review & editing, Supervision, Methodology, Conceptualization. **Fengfeng Li:** Supervision, Resources, Methodology,

Funding acquisition. **Chengjun Zeng:** Resources, Methodology, Investigation. **Wei Zhao:** Resources, Methodology, Investigation. **Liwu Liu:** Supervision, Resources, Project administration. **Yanju Liu:** Resources, Funding acquisition. **Jinsong Leng:** Writing – review & editing, Supervision, Resources, Project administration, Funding acquisition.

Declaration of competing interest

The authors declare that they have no known competing financial interests or personal relationships that could have appeared to influence the work reported in this paper.

Acknowledgments

This work was supported by the National Natural Science Foundation of China [grant number 12102107]; the China National Postdoctoral Program for Innovative Talents [grant number BX2021090]; the National Key R&D Program of China [grant number 2022YFB3805700]; and the Self-Planned Task of Songjiang Laboratory, Harbin Institute of Technology [grant number SL20230101].

Appendix A. Supplementary material

Supplementary data to this article can be found online at <https://doi.org/10.1016/j.compositesa.2025.108885>.

Data availability

Data will be made available on request.

References

- [1] Leng J, Lan X, Liu Y, Du S. Shape-memory polymers and their composites: Stimulus methods and applications. *Prog Mater Sci* 2011;56(7):1077–135.
- [2] Xia Y, He Y, Zhang F, Liu Y, Leng J. A review of shape memory polymers and composites: mechanisms, materials, and applications. *Adv Mater* 2021;33(6):e2000713.
- [3] Zhang F, Wen N, Wang L, Bai Y, Leng J. Design of 4D printed shape-changing tracheal stent and remote controlling actuation. *Int J Smart Nano Mater* 2021;12(4):375–89.
- [4] Li W, Liu Y, Leng J. Light-actuated reversible shape memory effect of a polymer composite. *Compos A Appl Sci Manuf* 2018;110:70–5.
- [5] Zhang D, Liu L, Lan X, Li F, Liu Y, Leng J. Experimental study on nonlinearity of unidirectional carbon fibre-reinforced shape memory polymer composites. *Compos A Appl Sci Manuf* 2023;166:107372.
- [6] Park M, Kim Y, Hwang JO, Park JK. Shape recovery characteristics of shape memory epoxy composites reinforced with chopped carbon fibers. *Carbon Lett* 2019;29(3):219–24.
- [7] Yarali E, Baniassadi M, Baghani M. Numerical homogenization of coiled carbon nanotube reinforced shape memory polymer nanocomposites. *Smart Mater Struct* 2019;28(3).
- [8] Li F, Scarpa F, Lan X, Liu L, Liu Y, Leng J. Bending shape recovery of unidirectional carbon fiber reinforced epoxy-based shape memory polymer composites. *Compos Appl Sci Manuf* 2019;116:169–79.
- [9] Korotkov R, Vedernikov A, Gusev S, Alajarmeh O, Akhatov I, Safonov A. Shape memory behavior of unidirectional pultruded laminate. *Compos A Appl Sci Manuf* 2021;150:106609.
- [10] Ren H, Ouyang Y, Xiao S, Xu W, Liu Y. Shape memory property and mechanism of the knitting-fabric reinforced epoxy composites subjected to tensile loading. *Compos Sci Technol* 2022;230:109764.
- [11] Ming GQ, Liu LW, Liu YJ, Leng JS. Space deployable parabolic reflector based on shape memory polymer composites. *Compos Struct* 2023;304:116327.
- [12] Zeng C, Liu L, Du Y, Yu M, Xin X, Liu T, et al. A shape-memory deployable subsystem with a large folding ratio in China's Tianwen-1 mars exploration mission. *Engineering* 2023;28:49–57.
- [13] Gong Y, Song Z, Ning H, Hu N, Peng X, Wu X, et al. A comprehensive review of characterization and simulation methods for thermo-stamping of 2D woven fabric reinforced thermoplastics. *Compos B Eng* 2020;203:108462.
- [14] Zhang D, Liu L, Xu P, Zhao Y, Li Q, Lan X, et al. Ancient papyrus scroll-inspired self-deployable mechanism based on shape memory polymer composites for Mars explorations. *Compos Struct* 2023;304:116391.
- [15] Ming G, Chen S, Li B, Li F, Liu L, Liu Y, et al. Design, fabrication and experimental verification of a drag sail based on thermal-driven controllable bi-stable shape memory polymer composite booms. *Smart Mater Struct* 2024;33(5):055040.
- [16] Liu Z, Lan X, Bian W, Liu L, Li Q, Liu Y, et al. Design, material properties and performances of a smart hinge based on shape memory polymer composites. *Compos B Eng* 2020;193:108056.
- [17] Fang G, Qu P, Cao Z, Shi F. Mechanical analysis of woven composites through experimental investigation and multiscale numerical simulation. *Fibers Polym* 2022;23(5):1440–53.
- [18] Li X, Qu P, Kong H, Zhu Y, Hua C, Guo A, et al. Multi-scale numerical analysis of damage modes in 3D stitched composites. *Int J Mech Sci* 2024;266:108983.
- [19] Qu P, Fang G, Kong H, Cao Z, Ma J, Wang Z, et al. Effect of thread count on the shear mechanical properties and dynamic mechanical properties of shape memory polymer reinforced by single-ply weave fabric. *Fibers Polym* 2023;24(9):3299–317.
- [20] Khan MA, Mabrouki T, Vidal-Sallé E, Boisse P. Numerical and experimental analyses of woven composite reinforcement forming using a hypoelastic behaviour. application to the double dome benchmark. *J Mater Process Technol* 2010;210(2):378–88.
- [21] Peng X, Rehman ZU. Textile composite double dome stamping simulation using a non-orthogonal constitutive model. *Compos Sci Technol* 2011;71(8):1075–81.
- [22] Zakertabrizi M, Hosseini E, Fallahi H, Creasy T, Tabei A, Razmjou A, et al. Dissecting atomic interweaving friction reveals the orbital overlap repulsion and its role in the integrity of woven nanofabrics in composites. *Adv Compos Hybrid Mater* 2024;7(3):86.
- [23] Kim W, Lee HE, Kim WT, Jo H, Kim SS. Effects of yarn interlacement in diamond triaxial braid on its patterns and tensile properties. *Compos Sci Technol* 2024;254:110678.